Retrieval and analysis of land surface microwave emissivity from SSM/I data

Nazzareno Pierdicca[1], Luca Pulvirenti[1], Christian Bignami[1], Marco Chini[2] and Francesca Ticconi[1]

[1]Dip. di Ingegneria Elettronica, Univ. "La Sapienza" di Roma, via Eudossiana 18 - 00184 Roma, Italy.
E-mail: pulvirenti@die.uniroma1.it
[2]Dip di Fisica, Univ. "Alma Mater Studiorum" di Bologna, viale Berti-Pichat 8 - 40127 Bologna, Italy

Abstract

The retrieval of land surface emissivity from microwave radiometric measurements is useful for monitoring the surface properties without being affected by the contribution of the atmosphere, which can be significant at higher frequencies. It is based on the inversion of the radiative transfer equation, assuming the absence of scattering phenomena. In this work, a method to improve the accuracy of the emissivity estimates through the removal of the effects of the atmosphere from the radiometric data and through the consideration of the surface elevation information is proposed. We have used the Special Sensor Microwave/Imager (SSM/I) observations over Italy throughout 1995. The atmospheric parameters have been derived from the NCEP vertical profiles, whilst the presence of clouds has been detected through METEO-SAT images co-located with the SSM/I ones. The data provided by a digital elevation model (DEM) have been also exploited. Monthly average maps of microwave emissivity relative to a geographical area including Italy have been produced to assess the whole estimation procedure, as well as to give examples of monitoring the seasonal trend of this parameter in a mountainous zone (Alps) and in a flat area (Po Plain).

Keywords: microwave radiometry, land emissivity

Riassunto

La stima dell'emissività superficiale da misure radiometriche a microonde è utile per monitorare le proprietà della superficie rimuovendo l'effetto dell'atmosfera che può essere significativo alle frequenze più alte. Essa si basa sull'inversione dell'equazione del trasferimento radiativo, supponendo in genere assenti fenomeni di diffusione. In questo lavoro viene proposto un metodo per migliorare l'accuratezza delle stime dell'emissività superficiale attraverso la rimozione degli effetti dell'atmosfera dal dato radiometrico e considerando l'informazione riguardante l'elevazione del terreno. Abbiamo considerato le osservazioni dello Special Sensor Microwave/Imager (SSM/I) sull'Italia nel 1995. I parametri atmosferici sono stati dedotti dai profili verticali NCEP, mentre la presenza di nubi è stata rivelata per mezzo di immagini METEOSAT co-locate con quelle SSM/I. Sono stati inoltre sfruttati i dati forniti da un modello digitale di elevazione del terreno (DEM). Sono state prodotte mappe mensili di emissività a microonde relative ad un'area geografica comprendente l'Italia per verificare la validità della procedura di stima e per fornire esempi di monitoraggio dell'evoluzione stagionale dell'emissività in una zona montuosa (Alpi) ed in una pianeggiante (Pianura Padana).

Parole chiave: radiometria a microonde, emissività del terreno

Introduction

Spaceborne microwave radiometry represents an important tool for the observation and the analysis of the Earth geophysical phenomena over a global scale. Microwave measurements are possible both during daytime and nighttime and present a greater penetration capability than that offered by higher frequencies (such as infrared bands), thus being sensitive to the internal characteristics of the surface (moisture, density, soil below vegetation, etc.).

Although the spatial resolution of microwave passive instruments (tens of kilometers) is coarse with respect to the small scale spatial variability of surface properties, estimating microwave land emissivity is of major interest [Prigent et al., 1997]. In fact, it represents the fundamental parameter to monitor land cover variations, vegetation and snow cover properties at regional or continental scale, without being affected by the atmosphere, which can considerably influence the radiometric measurements. Conversely, in atmospheric applications of microwave radiometry, singling out the surface background contribution and removing its effect from radiometric data has a considerable impact on the quality of the estimates of the meteorological parameters of interest (water vapor, precipitation amount, etc.) [Pulvirenti et al., 2002].

Many investigations have been carried out in the past decades to understand the mechanism responsible of the emission of soil and vegetation and to set up methods for estimating biogeophysical parameters from microwave radiometric measurements. Most of the studies have focused on the development of simple indices, obtained by combining the measurements at the different available radiometric channels, such as the Microwave Vegetation Index (*MVI*) proposed by Choudhury and Tucker [1987]. The use of these indices frequently aimed at compensating and possibly canceling the effects of nuisance parameters (namely, the atmospheric ones) on the radiometric observations. Attempts to evaluate land microwave emissivity have been accomplished in the study performed by Wilke and Mc Farland [1986], in which the emissivity has been assumed equal to the ratio between the measured brightness temperature (T_B) and the air physical temperature, thus supposing a transparent atmosphere, and in the work of Grody [1983].

The possibility to estimate land microwave emission from satellite radiometric data has been definitively demonstrated by the investigations of Prigent et al. [1997], [1998] and of Jones Andrew and Vonder Haar [1997]. They used microwave and infrared data, as well as atmospheric parameters derived from the National Center for Environmental Prediction (NCEP) analyses or radiosoundings. The infrared data have been used to derive the surface temperature and to detect cloud-free conditions.

In this work, we propose a method to improve the accuracy of the emissivity estimates from satellite microwave data and we apply it to the Special Sensor Microwave/Imager (SSM/I) observations over Italy throughout 1995 provided by the F11 platform. With respect to the works mentioned above, it can be used not only in cloud-free conditions, but also in the presence of non-scattering clouds. Moreover, our procedure exploits a low-resolution digital elevation model (DEM) to increase the accuracy of the data concerning surface temperature and atmospheric radiative parameters.

In order to assess the method, monthly average emissivity maps of Italy have been produced and their correspondence with the well-known characteristics of the Italian territory has been verified. Furthermore, these maps have permitted us to monitor the seasonal evolution of surface emissivity in a mountainous zone (Alps) and in a flat area (Po Plain).

Estimation method

As it was done by Prigent et al. [1998], our estimation procedure is based on the inversion of the radiative transfer equation. The T_B observed by a spaceborne radiometer results from

several contributions: the surface emission attenuated by the atmosphere, the downwelling atmospheric radiation (T_{DN}) reflected by the terrain and attenuated by the atmosphere and the upwelling atmospheric radiation (T_{UP}). The cosmic contribution can be neglected at the SSM/I frequencies. Indicating with T_s the surface temperature, with e_p the surface emissivity (p represents the polarization, either vertical or horizontal), with υ the frequency and with θ the observation angle, for a plane-parallel atmosphere in the absence of scattering phenomena, T_B can be expressed as:

$$T_{Bp}(\upsilon,\vartheta) = [e_p(\upsilon,\vartheta)T_s + T_{Bpsc}(\upsilon,\vartheta)]e^{-\tau_\upsilon(z_0,H)/\mu} + T_{UP}(\upsilon,\vartheta) \tag{1}$$

In Equation [1], T_{Bpsc} represents the fraction of T_{DN} scattered by terrain, $\tau_\upsilon(z_1,z_2)$ is the atmospheric optical thickness at nadir between the heights z_1 and z_2, μ is the cosine of the observation angle, H indicates the satellite altitude and z_0 denotes the surface height of the considered pixel. The latter has been derived in our procedure from a DEM. The parameter τ_υ is a function of the absorption coefficient k_a:

$$\tau_\upsilon(z_1,z_2) = \int_{z_1}^{z_2} k_a(\upsilon,z)dz \tag{2}$$

where z indicates the height. By assuming again the absence of scattering phenomena, the atmospheric temperatures can be expressed as:

$$T_{DN}(\upsilon,\vartheta) = \frac{1}{\mu}\int_{z_0}^{\infty} k_a(\upsilon,z)T(z)e^{-\tau_\nu(z_0,z)/\mu}dz = T_{mrDN}[1 - e^{-\tau_\nu(z_0,H)/\mu}] \tag{3}$$

$$T_{UP}(\upsilon,\vartheta) = \frac{1}{\mu}\int_{z_0}^{H} k_a(\upsilon,z)T(z)e^{-\tau_\nu(z,H)/\mu}dz = T_{mrUP}[1 - e^{-\tau_\nu(z_0,H)/\mu}] \tag{4}$$

In the Equations [3] and [4], T_{mrDN} and T_{mrUP} are the mean radiative temperatures associated to the downwelling and upwelling radiation, respectively. They can be defined as the temperatures that an isothermal atmosphere should have to be equivalent to the actual one. The mean radiative temperatures, together with the optical thickness τ_υ, completely describe the radiative behavior of the atmosphere and are related to the entire vertical profiles of the atmospheric temperature and composition.
An approximation that is suggested in many studies to considerably reduce the complexity of the calculations consists of supposing that the radiation scattered by the land surface has only the specular component:

$$T_{Bpsc}(\upsilon,\vartheta) = \left[1 - e_p(\upsilon,\vartheta)\right]T_{DN}(\upsilon,\vartheta) \tag{5}$$

By adopting this simplification, it is possible to invert Equation [1] and by substituting in [1]

the relationships given in [3], [4] and [5], a formula for the surface emissivity can be derived, starting from a given radiometric measurement $T_{Bp}(\upsilon, \theta)$:

$$e_p(\upsilon,\vartheta) = \frac{T_{Bp}(\upsilon,\vartheta) - \left[T_{mrDN}(\upsilon,\vartheta)\cdot e^{-\tau_\upsilon(z_0,A)/\mu} + T_{mrUP}(\upsilon,\vartheta)\right]\cdot\left(1 - e^{-\tau_\upsilon(z_0,A)/\mu}\right)}{\left[T_S - T_{mrDN}(\upsilon,\vartheta)\cdot\left(1 - e^{-\tau_\upsilon(z_0,A)/\mu}\right)\right]\cdot e^{-\tau_\upsilon(z_0,A)/\mu}} \qquad [6]$$

To determine the atmospheric parameters which are present in Equation [6], *i.e.*, mean radiative temperatures and optical thickness, we have applied a radiative transfer scheme, based on the gas absorption model developed by Liebe et al., [1993], to the atmospheric vertical profiles of pressure, temperature and relative humidity provided by "The NCEP/NCAR 40-year reanalysis project" [Kalnay et al., 1996] and furnished by the National Center for Environmental Prediction and the National Center for Atmospheric Research (NCEP/NCAR). The NCEP/NCAR data are available all over the Earth surface, with a spatial resolution of 2.5° both in longitude and in latitude and are relative to the synoptic hours (00:00, 06:00, 12:00, 18:00 GMT). The number of vertical layers is equal to 17, starting from the height corresponding to an atmospheric pressure of 1000 mbar. The different spatial resolution and geographic position between SSM/I pixel centers and NCEP grid points has been taken into account by computing T_{mrUP}, T_{mrDN}, τ and T_s at each SSM/I pixel location through a bilinear interpolation that considers the four NCEP grid points surrounding the pixel itself.

Equation [6] has been applied to each pixel of every SSM/I image provided by the F11 platform throughout the year 1995 over the Italian territory. The images have been furnished by NOAA/NESDIS and NOAA/FNMOC. SSM/I is mounted on a polar satellite which flies at about 900 km of altitude and measures the T_B at 19.35, 37.0 and 85.5 GHz in both horizontal and vertical polarization and at 22.2 GHz in vertical polarization only. The spatial resolution ranges from about 70 km for the 19 GHz channels to 15 km for the 85 GHz ones. More details about this sensor can be found in Hollinger et al., [1990].

As mentioned in the introduction, a distinctive characteristic of our procedure consists of the possibility to consider situations in which non-scattering clouds are present. For each SSM/I overpass, the temporarily closest (within ± 15 min) METEOSAT image has been collected. Then, a co-location procedure has been performed to carry out a joint analysis of microwave and METEOSAT images. The cloud detection has been performed by examining the METEOSAT images and by applying an unsupervised clustering algorithm [Tou and Gonzalez, 1974] to separate cloudy and cloud-free pixels. The clouds producing scattering effects have been discarded (and the corresponding pixels have been excluded from the computation of the monthly average maps) by using the Scattering Index (*SI*) developed for the SSM/I radiometer by Ferraro and Marks [1994]. They claimed that when *SI* exceeds 5-10 K, a potential scattering area is identified. We have adopted a conservative choice by selecting a maximum value equal to 5 K as indicative of the absence of scattering phenomena.

The effect of the non-scattering clouds, detected by the joint analysis described above, has been accounted for through the estimation of the cloud liquid density accomplished by adopting the model proposed by Decker et al. [1978] applied to the NCEP profiles and the corresponding computation of the cloud absorption coefficient. The Decker model firstly detects the presence of a cloud if the relative humidity of a given level of a vertical profile exceeds a threshold (*i.e.*, the critical humidity, that we have assumed equal to 95%) and then computes the liquid density as a function of the cloud thickness.
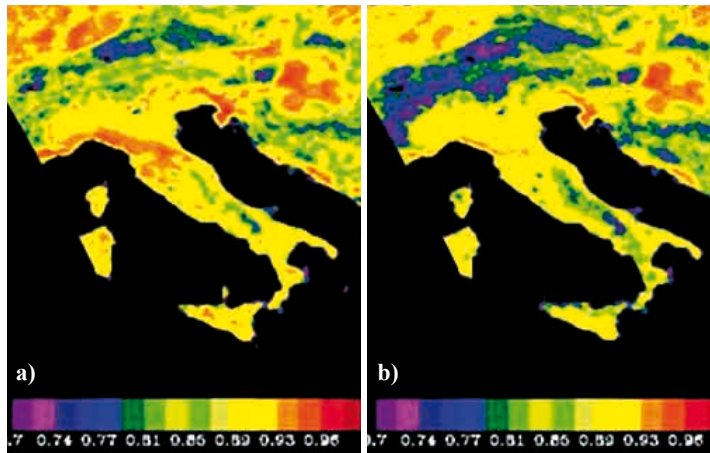
Figure 1 - Emissivity map derived from a single SSM/I image with (panel a) and without (panel b) exploiting the information of the surface elevation of every pixel provided by the digital elevation model (DEM). It concerns the 85 GHz, horizontal polarization channel.

Another distinctive characteristic of our procedure is represented by the use of the information regarding the surface elevation of every pixel of a SSM/I image. This is needed since the atmospheric radiative parameters depend on the surface height. Neglecting the information of the pixel height corresponds to put $z_0 = 0$ in Equations [1], [3] and [4] for all the SSM/I pixels. This implies the computation of the atmospheric parameters along a vertical column whose extension is generally greater than the actual one, thus yielding inaccurate emissivity estimates. Furthermore, we have approximated T_s with the air temperature at the same height, thus making $T_s = T_s(z_0)$. In a different context, the influence of surface elevation in evaluating atmospheric effects has been already accounted for in Schiavon et al. [1998]. METEOSAT thermal infrared channel could be useful to estimate the skin surface temperature, but the inclusion of the cloudy situations in our procedure prevents the systematic use of infrared data to derive T_s.

As mentioned, the surface elevation of every pixel of a SSM/I image has been derived from a DEM with resolution equal to 0.083° both in longitude and in latitude. Because of the different resolution of the SSM/I, an average value of the height has been considered for each radiometric pixel. To determine the surface values of the meteorological variables of interest, a vertical interpolation/extrapolation of the profiles has been carried out, since the lowest level of the NCEP data correspond to a pressure of 1000 mbar. As for T_s, a linear interpolation of the lowest two levels has been accomplished, whereas, for the surface humidity, we have assumed it equal to that at the lowest NCEP level. Regarding the atmospheric pressure, we have performed an exponential fitting of the lowest three values. Figure 1 shows an example, relative to one SSM/I image (85 GHz, horizontal polarization) of an emissivity map derived with (panel a) and without (panel b) exploiting the DEM data. The difference is evident in mountainous areas and can be ascribed to the atmosphere. In fact, in this case, without exploiting the DEM data, the atmospheric attenuation is overestimated thus implying underestimation of the emissivity of the surface background.

Analysis of the results

The results of the procedure described above are presented as monthly average emissivity maps relative to an area including Italy (36°-50° N, 5°-20° E). As mentioned, they are relative to year 1995 and they have been derived by processing 717 SSM/I images (both ascending and descending passes). For every SSM/I pixel we have calculated the emissivity
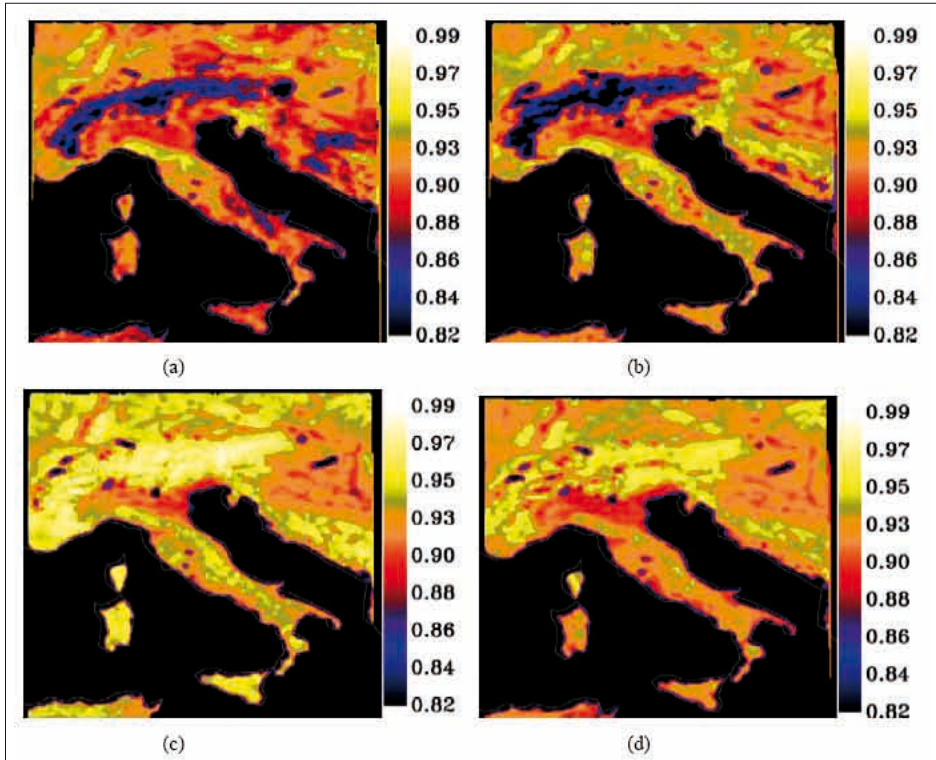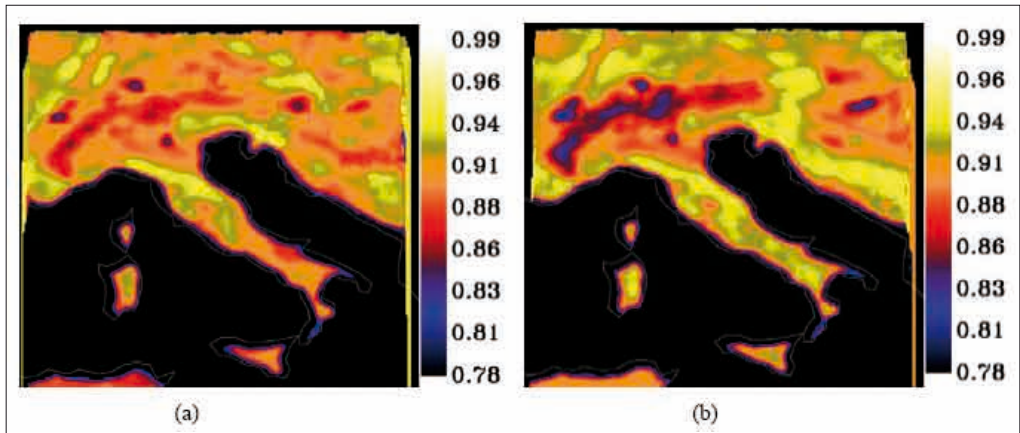
**Figure 2 - Monthly average emissivity maps for the 85 GHz, horizontal polarization channel.
Panel a: January 1995; panel b: March 1995; panel c: July 1995; panel d: October 1995.**

according to Equation [6] and, to produce the maps, all these emissivity values have been projected over a 0.0625x0.0625 degrees regular grid and, successively, averaged. Note that not all the SSM/I data are converted into emissivity values, since pixels affected by atmospheric scattering have been discarded.

We emphasize that the following considerations do not intend to interpret in detail the characteristics of the maps since neither ground truth data, nor modeling tools are used in this work. They only aim at giving examples of the types of information that can be extracted from the maps.

Figure 2 shows the maps obtained for the 85 GHz, horizontal polarization channel (85H). They concern the months of January (panel a), March (panel b), July (panel c) and October (panel d). The first characteristic clearly detectable is the presence of the snow in the Alpine region (panels a and b), which on the maps corresponds to the areas in which the emissivity is low (less than 0.88). At the SSM/I frequencies, the emissivity of the snow is less than that characteristic of land and vegetation, except for very wet snow [Bauer and Grody, 1995].

In the maps regarding January and March we can observe the presence of black zones in which the 85H emissivity (e_{85H}) is low and blue areas in which it is slightly higher. The former correspond to values equal to 0.82-0.83 in January and smaller (less than 0.80) in March (note that the maps are saturated to a minimum equal to 0.82 for the sake of figure clarity). The blue areas in the Alpine region correspond to $e_{85H} = 0.85$-0.86. It is worth mentioning that the possible confusion with lakes (also characterized by a small emissivity) that
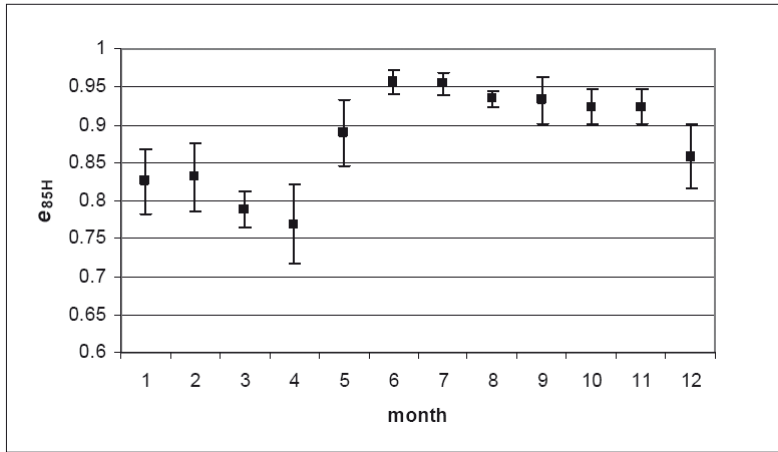
Figure 3 - Monthly average emissivity maps for the 37 GHz, horizontal polarization channel. Panel a: January 1995; panel b: March 1995.

may arise from the observations of Figure 2a, b can be easily overcome by examining the maps of the polarization difference (not shown for the sake of conciseness), which is higher for the water bodies.

As for January 1995, in the black areas we can deduce the presence of dry snow, that presents a decrease of the emissivity due to ice-scattering [Bauer and Grody, 1995]. It is worth mentioning that the dark area in the Eastern Alps (see Fig. 2a) shows very low values (around 0.76). However, for this area only two SSM/I images have been included in the computation of the monthly average, because of a persistent coverage of scattering clouds, so that the emissivity evaluation is unreliable. The blue areas in Figure 2a indicate the probable presence of wetter snow, characterized by a higher emission with respect to dry snow, determined by the higher absorption. As far as March 1995 is concerned, there is a reduction of the area covered by snow in the Eastern regions (and in the Apennine zone), but an increase in Western and Central Alps. The decrease of the emissivity with respect to January, which is not revealed by Figure 2 for the saturation to 0.82, is visible in Figure 3 that concerns the 37H channel (panel a: January; panel b: March). We can explain this decrease by supposing that the snow depth in March is larger than that occurring in January and that, in addition, in March the refrozen snow, characterized by a series of processes of melting and freezing that give rise to strong scattering phenomena, tends to reduce the emissivity.

To further analyze the seasonal variation of the emissivity in the Alpine region, Figure 4 shows the monthly trend of the mean value plus and minus the standard deviation of e_{85H} for a single pixel (whose location is 44.79° N, 6.34° E). The presence of dry snow in the first winter months (January and February) and of refrozen snow in March and especially in April seems to be confirmed. The large standard deviation in April can be due both to refrozen snow and to the progressive disappearance of the snow cover. Note that we have included in our computations both day and night satellite overpasses, so that the standard deviation reflects also the variation due to the diurnal cycle. In the following months, snow disappears from the Alpine region and the emissivity reaches higher values especially in July (see Fig. 2c).

This derives from a combination of effects caused by surface roughness and by the appearance of vegetation, in particular the coverage of snow-free coniferous forests and the increasing biomass of deciduous forests. The combined effect of roughness and vegetation

Figure 4 - Mean value plus/minus standard deviation of the monthly average emissivity at 85 GHz, horizontal polarization for a pixel in the Alpine region (44.79°N, 6.34°E).
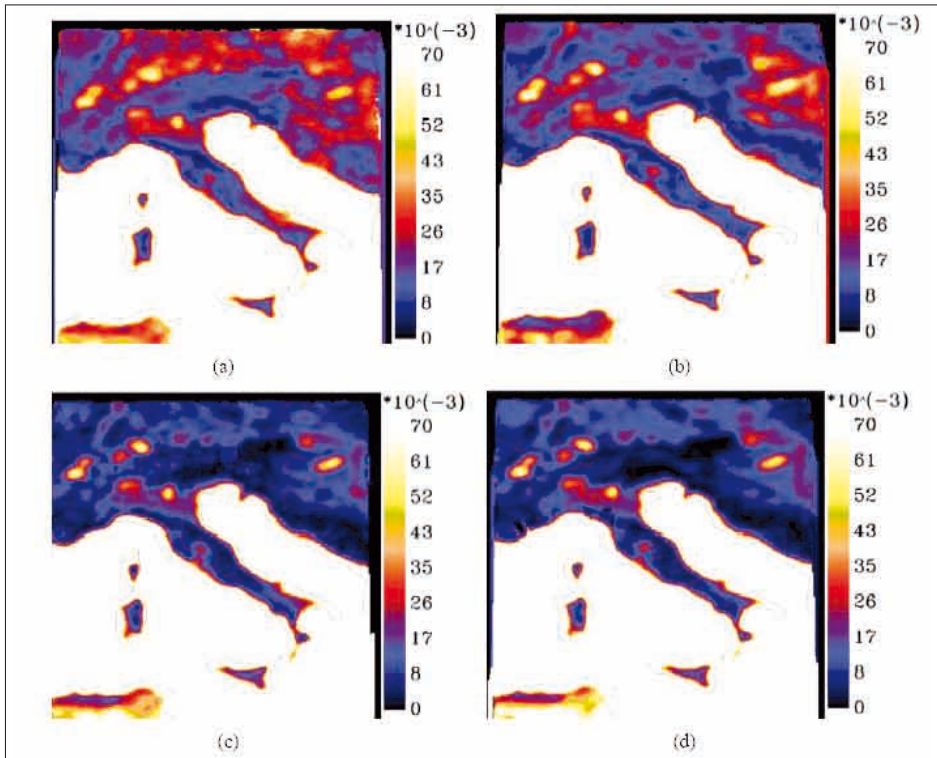
Figure 5 - Monthly average maps for the difference between 37 GHz emissivities at vertical and horizontal polarization. Panel a: January 1995; panel b: March 1995; panel c: July 1995; panel d: October 1995.

cover and growth is visible also for the Apennine area in Figures 2a (in which the presence of snow can be detected too), 2b and 2c.

From the observation of Figure 2, the zone corresponding to the Po Plain can be distinguished (red area southwards the Alps in Fig. 2a). A plain bare soil presents values of difference between the emissivities at vertical and horizontal polarizations (Δe) higher than those characteristic of vegetation covered areas. Figure 5 shows Δe_{37} for the four months considered in Figure 2. It can be observed that Δe_{37} in the Po plain is high in March, when values greater than 30×10^{-3} are reached, an low in July for which values less than 10×10^{-3} are found.

To better analyze the seasonal behavior of the emissivity in the Po plain, Figure 6 shows, in panel a, the monthly trend of the mean value of Δe_{19} for a single pixel (whose location is 44.94° N, 11.00° E). Panel b shows the trend of the mean value plus and minus the standard deviation of e_{19H} for the same pixel. As for Δe_{19}, it is maximum in March and minimum in July. A possible explanation for the presence of the maximum in March might be: a still low level of vegetation growth, combined with high values of soil moisture, since a wet bare soil is characterized by lower T_B's and higher values of polarization differences with respect to dry soils. This occurs particularly at lower frequencies (this is the reason why we are considering the 19 GHz band in this case) more sensitive to soil moisture, for which the emissivity at horizontal polarization strongly decreases at lower frequencies, as reported by Bauer and Grody, [1995].

As for e_{19H}, it follows the vegetation cycle (see Fig 6b). It increases during spring (reaching its maximum in May) and then it tends to decrease. It is interesting to note that the standard deviation of the emissivity at 19 GHz is generally larger, except for the summer months, than that at 85 GHz (not shown for the sake of conciseness) in the Po plain. The low variability of the emissivity at 85 GHz indicates that the removal of the atmospheric effects has been correctly performed, since the 85 GHz channels are the most sensitive to the atmosphere.

This is confirmed also by Figure 4 (concerning Alps) which shows that, throughout the summer months in which there is not the influence of snow, the standard deviation of e_{85H} is small. At 19 GHz, that is the channel less sensitive to the atmosphere, little of the variability is explained by clouds or changes in water vapor content, whereas it is related to modifications of soil characteristics (e.g., soil moisture).
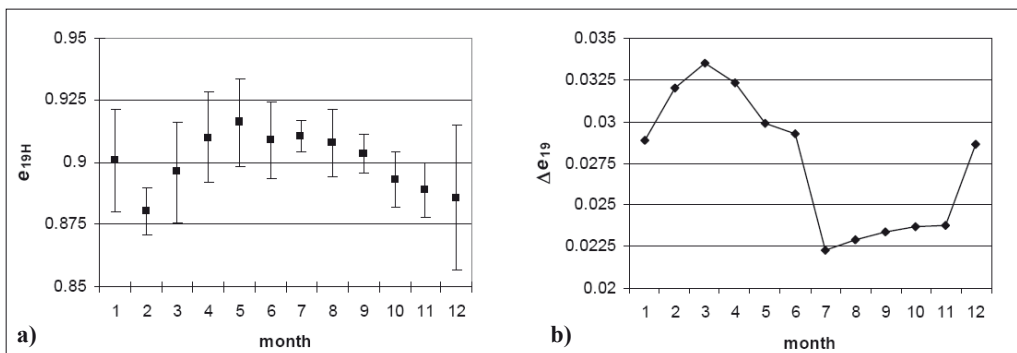
Figure 6 - Panel a: difference between 19 GHz emissivities at vertical and horizontal polarization for the same pixel. Panel b: mean value plus/minus standard deviation of the monthly average emissivity at 19 GHz, horizontal polarization for a pixel in the Po Plain (44.94° N, 11.00° E).

It is interesting to compare our results for the Po plain with those obtained in a past investigation employing the same sensor, which used data acquired throughout 1987-1988 [Amodeo et al., 1997]. The fairly large values of Δe_{19} that we have found in spring and the quite small values in autumn do not fully agree with the results of Amodeo et al., whilst, also in the latter study, the minimum of the polarization difference has been found in summer. The discrepancies can be ascribed again to variations of soil moisture content, strictly correlated to the precipitation amount. It is worth mentioning that in a more recent study exploiting the data, acquired throughout 2002-2003, from the Advanced Microwave Scanning Radiometer for the Earth Observing System (AMSR-E) [Santi et al., 2005], a high value of the polarization difference at 19 GHz in the Po plain has been found in spring (May 2003).

Conclusions

A procedure to estimate surface emissivity from spaceborne microwave radiometric measurements has been presented. It is founded on the radiative transfer equation in absence of scattering phenomena and it uses auxiliary data, that is NCEP vertical atmospheric profiles and METEOSAT images in order to remove the effects of non-scattering clouds and of the atmosphere itself. With respect to previous works, it computes the emissivity in cloudy conditions too and it includes the information about the height of a pixel provided by a Digital Elevation Model to improve the accuracy of the emissivity estimates. Our results have been presented in form of monthly emissivity maps relative to a geographical area including Italy. From the analysis of these maps the capability to detect the presence of different kinds of snow and to monitor the growth of the vegetation has emerged.

References

Amodeo G., Macelloni G., Paloscia S., Susini C. (1997) - *L'uso dello SSM/I nello studio delle caratteristiche del territorio europeo.* Riv. It. Teleril., 9: 23-34.

Bauer P., Grody N. C. (1995) - *The potential of combining SSM/I and SSM/T2 measurements to improve the identification of snowcover and precipitation*. IEEE Trans. Geosci. Remote Sensing, 33: 252-261.

Choudhury B. J., Tucker C. J. (1987) - *Monitoring global vegetation using Nimbus-7 37 GHz. Some empirical relations*. Int. J. Remote Sens., 8: 1085-1090.

Decker M. T., Westwater E. R., Guiraud F. O. (1978) - *Experimental evaluation of ground-based microwave radiometric sensing of atmospheric temperature and water vapor profiles*. J. Appl. Meteorol, 17: 1788-1795.

Ferraro R.R., Marks G. F. (1994) - *Effects of surface conditions on rain identification using the SSM/I.* Rem. Sens. Rev., 11: 195-209.

Grody N. C. (1983) - *Severe storm observations using the Microwave Sounding Unit*. Journal of Climatology and Applied Meteorology, 22: 609-625.

Hollinger P., Peirce J. L., Poe G.A. (1990) - *SSM/I instrument evaluation.* IEEE Trans. Geosci. Remote Sens., 28: 781-790.

Jones Andrew S., Vonder Haar T. H. (1997) - *Retrieval of microwave surface emittance over land using coincident microwave and infrared satellite measurements*. Journal of Geophysical Research, 102: 13.609-13.626.

Kalnay E. et al. (1996) - *The NCEP/NCAR 40-year reanalysis project.* Bulletin of the American Meteorological Society, 77: 437-470.

Liebe H.J., Hufford G. A., Cotton M. G. (1993) - *Propagation modeling of moist air and suspended water/ice particles at frequencies below 1000 GHz*. AGARD Conf. Proc. 542.

Prigent C., Rossow W. B., Matthews E. (1997) - *Microwave land surface emissivities estimated from SSM/I observations*. Journal of Geophysical Research, 102: 21.867-21.890.

Prigent C., Rossow W. B., Matthews E. (1998) - *Global maps of microwave land surface emissivities: Potential for land surface characterization.* Radio Science, 33: 745-751.

Pulvirenti L., Pierdicca N., Marzano F. S., Castracane P., D'Auria G. (2002) - *A Physical-Statistical Approach to Match Passive Microwave Retrieval of Rainfall to Mediterranean Climatology.* IEEE Trans. Geosci. Remote Sens., 40: 2271-2284.

Santi E., Macelloni G., Paloscia S. (2002) - *Multitemporal Analysis of AMSR-E Data: A Large Scale Monitoring of Earth's Surface Parameters.* Proc. IEEE/IGARSS 2005, 5: 3466- 3469.

Schiavon G., Ferrazzoli P., Solimini D., de Maagt P.. Poiares Baptista J.P.V. (1998) - *A global high-resolution microwave emission model for the Earth.* Radio Science, 33: 753-766.

Tou J. T., Gonzalez R. C. (1974) - *Pattern Recognition Principles.* Addison-Wesley Publishing Company, Reading, Massachusetts.

Wilke G. D., Mc Farland M. J. (1986) - *Correlation between Nimbus-7 scanning multichannel microwave radiometer data and an antecedent precipitation index.* Journal of Climatology and Applied Meteorology, 25: 227-238.